Title

Tracking Uptake and Metabolism of Xenometallomycins Using a Multi-Isotope Tagging Strategy.

Journal

ACS Infectious Diseases, 8(4)

Authors

Pandey, Apurva
Cao, Minhua
Boros, Eszter

Publication Date

2022-04-08

DOI

10.1021/acsinfecdis.2c00005

Peer reviewed

HHS Public Access

Author manuscript

ACS Infect Dis. Author manuscript; available in PMC 2022 June 01.

Published in final edited form as:

ACS Infect Dis. 2022 April 08; 8(4): 878–888. doi:10.1021/acsinfecdis.2c00005.

Tracking Uptake and Metabolism of Xenometallomycins Using a Multi-Isotope Tagging Strategy

Apurva Pandey,
Department of Chemistry, Stony Brook University, New York 11794, United States

Minhua Cao,
Department of Chemistry, Stony Brook University, New York 11794, United States

Eszter Boros
Department of Chemistry, Stony Brook University, New York 11794, United States;

Abstract

Synthetic and naturally occurring siderophores and their conjugates provide access to the bacterial cytoplasm via active membrane transport. Previously, we displaced iron with the radioactive isotope ^{67}Ga to quantify and track in vitro and in vivo uptake and distribution of siderophore Trojan Horse antibiotic conjugates. Here, we introduce a multi-isotope tagging strategy to individually elucidate the fate of metal cargo and the ligand construct with radioisotopes ^{67}Ga and ^{124}I. We synthesized gallium(III) model complexes of a ciprofloxacin-functionalized linear desferrichrome (Ga-**D6**) and deferoxamine (Ga-**D7**) incorporating an iodo-tyrosine linker to enable radiolabeling using the metal-binding (^{67}Ga) and the cargo-conjugation site (^{124}I). Radiochemical experiments with *Escherichia coli*, *Staphylococcus aureus*, and *Pseudomonas aeruginosa* wt strains show that ^{67}Ga-**D6**/**D7** and Ga-**D6**-^{124}I/**D7**-^{124}I have comparable uptake, indicating intact complex import and siderophore-mediated uptake. In naive mice, ^{67}Ga-**D6**/**D7** and Ga-**D6**-^{124}I/**D7**-^{124}I demonstrate predominantly renal clearance; urine metabolite analysis indicates in vivo dissociation of Ga(III) is a likely mechanism of degradation for ^{67}Ga-**D6**/**D7** when compared to ligand radiolabeled compounds, Ga-**D6**-^{124}I/**D7**-^{124}I, which remain >60% intact in urine. Cumulatively, this work demonstrates that a multi-isotope tagging strategy effectively elucidates the in vitro uptake, pharmacokinetics, and in vivo stability of xenometallomycins with modular chemical structures.

Graphical Abstract

Corresponding Author: Eszter Boros – Department of Chemistry, Stony Brook University, New York 11794, United States; eszter.boros@stonybrook.edu.

Supporting Information

The Supporting Information is available free of charge at https://pubs.acs.org/doi/10.1021/acsinfecdis.2c00005.

Synthesis and characterization of intermediates for the synthesis of **D6** and **D7**, representative HPLC traces of ligands and their corresponding complexes, MIC experiments, radiochemical characterization, radiochemical bacterial uptake data, and tabulated biodistribution data (PDF)

The Supporting Information is available free of charge on the ACS Publications website.

Complete contact information is available at: https://pubs.acs.org/10.1021/acsinfecdis.2c00005

The authors declare no competing financial interest.

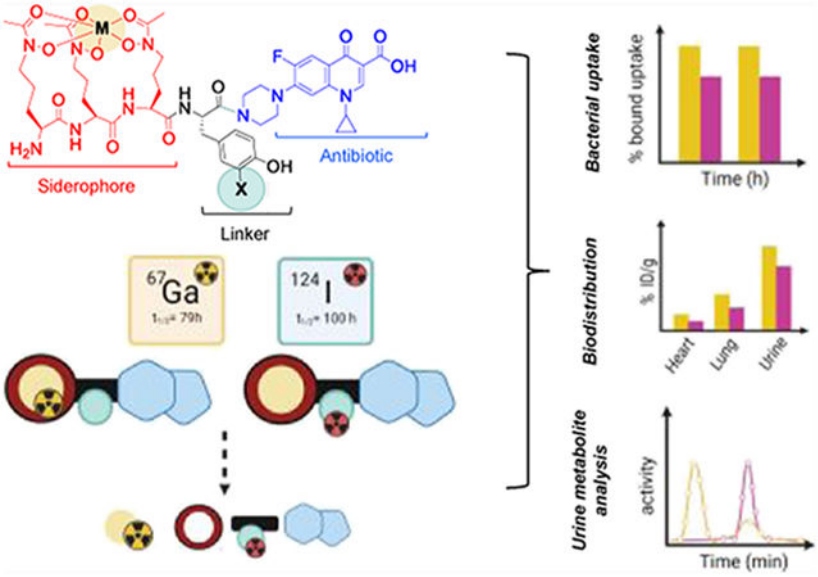

Keywords

siderophore; xenometallomycin; multi-isotope tagging; gallium-67; iodine-124; Trojan Horse antibiotic conjugates

Antibiotic resistance is one of the biggest public health challenges of recent times.[1] Bacterial resistance is emerging worldwide, diminishing the efficacy of established antibiotics. Among infective agents, the Gram-positive pathogens *Staphylococcus aureus* and *Streptococcus pneumoniae*, Gram-negative pathogens *Acinetobacter baumannii*, and *Enter-obacteriaceae* such as *Escherichia coli* cause the majority of US hospital acquired infections and deaths, with a growing number of resistance cases, as reported by the Centers for Disease Control and Prevention (CDC).[1,2] Bacterial strains have developed mechanisms to lower the permeability of their membranes toward antibiotics or express membrane efflux pumps to expel antibacterial small molecules before they can take action.[3–6] Overcoming these resistance mechanisms by taking advantage of bacterial nutrient uptake pathways is a well-established strategy, as siderophore antibiotic conjugates have been studied in detail in this regard.

These conjugates act as “Trojan Horses” and take advantage of the bacterial iron assimilation pathway to deliver antibiotics to the cytoplasm.[7–9] Miller,[10–15] Nolan,[16–20] Bronstrupp,[21] Duhme-Klair,[22–24] and Wencewicz[8,12,25] have demonstrated that this strategy is not only efficacious but also provides insights into the frequently complex bacterial iron acquisition pathways. Our group focuses on xenometallomycins, which are Trojan horse conjugates that incorporate a nonendogenous metal ion for co-delivery and to enhance bactericidal activity.[26,27] We hypothesize that nonendogenous metal ions can exert additional, metal-based toxicity, to further enhance compound potency and attenuate bacterial resistance. We have previously successfully validated this approach with siderophore antibiotic conjugates Ga-**D1**, Ga-**D2,** and Ga-**D5** (Figure 1), inspired by the structures of the natural product antibiotics salmycin and albomycin.[25–30] Our

constructs comprised three components: (1) the metal-bound siderophore, (2) a noncleavable linker, and (3) a fluoroquinolone-based antibiotic. Because of the peptidic nature of these constructs, sequence modification is synthetically tractable. Our previous work demonstrated that co-delivery of Ga(III), a redox inactive mimic of Fe(III), produces enhanced potency when compared with the *apo*-(metal free) or Fe-bound siderophore conjugate. Our first-generation lead construct Ga-**D2** (Figure 1) demonstrated low μM broad-spectrum potency in *E. coli* (*E. coli*), *S. aureus* (*S. aureus*), *P. aeruginosa,* and *Klebsiella Pneumoniae* (*K. pneumoniae*).[26] More recently, we demonstrated that the xenometallomycin concept can yield compounds that exceed the potency of the parent antibiotic in vitro and in vivo with the second-generation compound Ga-**D5** (Figure 1).[27] However, while synthetic siderophore antibiotic conjugates have been extensively explored, the structure–activity relationship remains difficult to predict. Furthermore, the exact mechanism of the antiproliferative activity of Ga(III) siderophore complexes is not well established and requires further study.

Current methods to elucidate the transport mechanisms of these constructs involve modulating the transport protein expression levels, followed by bacterial growth assessment in the presence of siderophores or siderophore antibiotic conjugates.[31–34] These methods cannot provide information on the efficiency of transport of individual components, the metabolic stability of constructs, and their potential for in vivo applications. Evidently, more specific and quantitative readouts are needed for characterizing siderophore-mediated metal-ion transport in vitro and in vivo.

The use of radioactive isotopes is very convenient in this regard. The feasibility of this approach was originally demonstrated by Raymond et al. using radioactive ^{14}C tag incorporation into siderophores during (bio)synthesis[35] and ^{55}Fe/^{59}Fe labeling to elucidate siderophore-mediated iron uptake pathways.[36–38] However, as complex thermodynamic stability and kinetic inertness differs based on the identity of the metal ion, it is crucial that radioisotopes are employed in accordance with the metal's identity within the compound of interest. While Decristoforo et al. have employed labeled siderophores for the targeted imaging of fungal infections with ^{68}Ga,[39–43] labeling of synthetic siderophore antibiotic constructs to elucidate in vitro uptake and in vivo pharmacokinetics has remained underutilized.

Here, we employ a multi-isotope tagging approach to elucidate the uptake, metabolism, and in vivo distribution of xenosiderophore antibiotic drug conjugates using short-lived, biomedical isotopes. The proposed radioactively labeled siderophore conjugates incorporate the following isotope tags (Figure 2): (1) a radioactive metal-ion cargo ^{67}Ga(III) ($t_{1/2}$ = 3.3 d, as a nonredox active Fe mimic) incorporated by coordinative binding to the siderophore structure (**M**) and (2) a tyrosine residue which enables incorporation of a covalent isotope tag (**X**) ^{124}I ($t_{1/2}$ = 4.2 d). Both isotopes have emission properties that enable noninvasive imaging with single photon emission computed tomography (SPECT; ^{67}Ga) or positron emission tomography (PET; ^{124}I).

Previously, we demonstrated that ^{67}Ga is suitable to study the biodistribution and pharmacokinetics of our first-generation siderophore antibiotic conjugates ^{67}Ga-**D1**, ^{67}Ga-

D2, and Ga-**D5** (Figure 1).[26,27] However, tracking of the metal ion alone does not provide information on other components of the conjugate.

To ameliorate this, we introduce ^{124}I as a complementary, covalent linker tag to track uptake and pharmacokinetics of the small molecule conjugate component.

The isotope ^{124}I is extensively utilized as a PET radiotracer. The 4.2 d half-life and high β energy ($E_{\beta^+(\max)}$ = 819 KeV) allows for time intensive radiosynthesis protocols and PET imaging studies.[44] A wide variety of compounds have been labeled for molecular imaging with PET. *m*-Iodobenzylguanidine (MIBG) is used in diagnosis (^{123}I or^{124}I) and therapy (^{131}I) of neuroblastoma and pheochromocytoma.[45,46] Small molecule tracers such as [^{124}I]Iodo-azomycin-galactopyranoside ([^{124}I]IAZG) have been studied as hypoxia imaging agents.[47–50] The uracil derivative [^{124}I]1-(2-deoxy-2-fluoro-1-d-arabinofuranosyl)-5-iodouracil has been reported as a PET radiotracer for noninvasive imaging of musculoskeletal bacterial infections.[51]

The use of mild chemical approaches that are compatible with hydrolytically labile gallium-siderophore coordination complexes disqualifies commonly used strategies that involve halogen exchange and the use of strong Lewis acids in organic solvents. However, radioiodination of peptides and proteins can be achieved under comparatively mild reaction conditions with reagents like Chloramine T, Iodogen, and various enzymatic approaches to introduce direct, electrophilic radiohalogenation of phenols.[52–55]

Here, we introduce two Trojan horse conjugates, **D6** and **D7** (Figure 1), as proof-of-concept constructs for the introduction of two complementary radiochemical tags to gallium-based xenometallomycins. We show that quantification of the individual radioisotope-tagged constructs in bacterial uptake assays successfully tracks the bacterial uptake of the different compound components (Figure 2) and informs the distribution and metabolism of each component in vivo. This provides insights to enable rational drug design of xenometallomycins.

RESULTS AND DISCUSSIONS

Synthesis of Siderophore Antibiotic Conjugates D6 and D7.

The structures of **D6** and **D7** (Figure 2) are based on natural products albomycin[28] and salmycin,[30] respectively, and resemble the previously studied **D1**, **D2,** and **D5** compound series. Both structures incorporate a tyrosine within the linker for facile tagging with the ^{124}I isotope.

We employed a synthetic strategy in accordance with our first-generation lead **D2** for the synthesis of **D6**. Precursor **P5** was synthesized following previously established protocols (see Supporting Information).[26,56,57] The final product **D6** was obtained in $a < 2\%$ overall yield after 16 steps. To synthesize **D7**, we employed desferrioxamine (DFO) as a commercially attainable surrogate of danoxamine and introduced tyrosine by adaptation of our previously published protocol.[26] The final product **D7** was isolated in $a < 6\%$ overall

yield after 5 steps (Scheme S2). Nonradioactive iodination with selectfluor and NaI was conducted to produce single-halogenated derivatives **D6-I** and **D7-I**.

Ga- and Fe-D6/D7 Complex Formation.

Complexation with Ga(III) and Fe(III) salts formed Ga-**D6/D7** and Fe-**D6/D7** in aqueous, buffered media at pH 6 and pH 7. Further purification of Ga(III) and Fe(III) using reversed-phase chromatography was carried out to isolate the white and orange-red complexes, respectively. The same procedure was used for **D6-I/D7-I** ligands. Characterization via high-performance liquid chromatography (HPLC), high-resolution mass spectrometry (HRMS), and inductively coupled plasmaoptical emission spectroscopy (ICP-OES) was employed to confirm purity and produce consistent complex concentrations for subsequent in vitro and in vivo studies based on the quantitation of metal content (Figures S5, S6, S16, S17, S23, S24, S35, and S36).

Growth Inhibition in *wt* Bacterial Strains.

With apo-(metal-free), Ga, and Fe complexes of **D6** and **D7** in hand, we next probed bacterial growth inhibition in a conventional minimum inhibitory concentration (MIC) assay under iron-limiting conditions.[20,58,59] *E. coli* K12 and *P. aeruginosa* PA01 were selected as Gram-negative model organisms, and *S. aureus* RN4220 as the Gram-positive model organism.

Results are summarized in Table 1 and Figures 3, S38, and S39. The parent drug ciprofloxacin was utilized as a control, giving an MIC of 0.93 μM, which is consistent with literature values. The *apo*-**D6** and *apo*-**D7** constructs showed an MIC at >30 μM in wt *E. coli*, whereas Ga-**D6** was determined to have an MIC at 1.9 μM and Ga-**D7** MIC of 30 μM in wt *E. coli*, indicating the loss of potency when compared with first-generation conjugates Ga-**D2** and Ga-**D1**, respectively (Figures S38A and S39A and Table 1). In accordance with our previous findings, Fe(III) complexes remain significantly less active when compared with *apo* and Ga(III) complexes (Figure S38A and Table 1).

In *P. aeruginosa*, none of the **D6** and **D7** compounds showed inhibitory activity. Ga-**D6** also exhibited reduced activity in *S. aureus* with an MIC of 3.8 μM comparable to its activity in wt *E. coli*.

Because of a lack of inhibitory activity at tested conditions in *PA01*, we assessed the MIC of iodinated compounds Ga-**D6**-I and Ga-**D7**-I only in *S. aureus* and *E. coli* strains. Ga-**D6**-I exhibited 5-fold and 10-fold reduced activity in *S. aureus* and *E. coli*, respectively, when compared to Ga-**D6**, whereas Ga-**D7**-I showed comparable activity to Ga-**D7** in *S. aureus* (Figure 3D, Table 1). Overall, our results indicate that the introduction of the tyrosine residue into the linker affects the antibiotic potency of Ga-**D6** and Ga-**D7** when compared to that of their parent compounds, Ga-**D1** and Ga-**D2**.

Radiochemical Labeling with ^{67}Ga.

The formation of the ^{67}Ga-**D6** and ^{67}Ga-**D7** complexes was feasible under mild radiolabeling conditions [pH 7, 100 mM N-(2-hydroxyethyl)-piperazine-*N*′-ethanesulfonic

acid (HEPES), 5 min] quantitatively with ligand concentrations of 10^{-6} M (Schemes S3 and S4). The complexation was monitored using a radio-HPLC (Figures S40 and S41). Radiolabeling of **D6**-I and **D7**-I with ^{67}Ga was conducted under identical conditions but produced the desired products with a lower overall radiochemical yield (~15%). To remove unlabeled precursors and carriers, chromatographic purification and isolation of all ^{67}Ga-**D6**-I and ^{67}Ga-**D7**-I conjugates were employed (Figures 4, S42), producing effective compound concentrations of approximately 10^{-8} M without the nonradioactive carrier.

Radiochemical Labeling with ^{124}I.

Iodination of Ga-**D6** and Ga-**D7** was achieved in plastic tubes precoated with 1,3,4,6-tetrachloro-3alpha,6alpha-diphenylglycouril (Iodogen), in accordance with commonly utilized procedures for peptide and antibody labeling. After 45 min incubation at room temperature, at ~5 mM ligand concentration, a radiochemical yield of 15% was achieved, which also required chromatographic purification of the desired product to reduce loading of the competing parent Ga-**D6** and Ga-**D7** complexes, which could impede bacterial uptake experiments significantly by reduction of specific activity (Figures 4 and S42). Isolated fractions were analyzed with radio-HPLC to affirm that purification and removal of the parent carrier was successful, producing effective compound concentrations of approximately 10^{-8} M without the nonradioactive carrier.

Radiochemical uptake experiments in *wt* bacterial strains. The radiolabeled ^{67}Ga-**D6**-I/**D7** complexes were used to probe time-dependent compound uptake and quantification with ^{67}Ga-citrate as the control. *E. coli*, *S. aureus*, and *P. aeruginosa* (3.2×10^8 cfu) were incubated in Fe-deficient bacterial growth media with 0.07 MBq (corresponding to 6.75×10^{-9} M effective, noncarrier added compound concentration) of ^{67}Ga-**D6**/**D7**-I at 37 °C and uptake was sampled at 10, 20, 30, 60, and 120 min. For all tested strains, ^{67}Ga-**D6**-I displayed reduced uptake when compared to the first-generation conjugate ^{67}Ga-**D2**, with a maximum uptake of 5, 7, and 13 for *E. coli*, *P. aeruginosa*, and *S. aureus* respectively at 2 h (Figures S43, S44, 5A, and Tables S1–S3). In addition, ^{67}Ga-**D7**-I also demonstrated decreased uptake in comparison to the first-generation ^{67}Ga-**D1**, with a maximum uptake of 3, 20, and 12% for *E. coli*, *P. aeruginosa,* and *S. aureus*, respectively, at 2 h (Figures S45 and 46, 5B, and Tables S4–S6). Our data suggest that the introduction of iodinated tyrosine reduces the uptake of ^{67}Ga-**D6**-I and ^{67}Ga-**D7**-I in most bacterial strains, likely due to reduced binding affinity to the siderophore transporters required for trafficking across the bacterial membrane. Results with ^{67}Ga-**D6** and ^{67}Ga-**D7** compared well with those with ^{67}Ga-**D6-I/D7**-I, indicating that an adverse effect is also produced by the incorporation of a regular tyrosine residue.

For ^{124}I uptake experiments, Ga-**D6**-^{124}I, Ga-**D7**-^{124}I, and Tyrosine-^{124}I (control) were prepared with a specific activity of 1.9 MBq/μmol. *E. coli*, *S. aureus*, and *P. aeruginosa* (3.2×10^8 CFU) were incubated in Fe-deficient growth media with 0.14 MBq of Ga-**D6**-^{124}I, 0.15 MBq (corresponding to 1.3×10^{-8} M effective, noncarrier added compound concentration) of Ga-**D7**-^{124}I and Tyrosine-^{124}I (control) at 37 °C in direct comparison to experiments conducted for ^{67}Ga-labeled conjugates. In *S. aureus*, we observed a good correlation of Ga-**D6**/**D7**-^{124}I uptake with those of ^{67}Ga-**D6/D7** and ^{67}Ga-**D6/D7**-I.

Uptake in *E. coli* and *P. aeruginosa* was decreased for all **D6** and **D7**-derivatives, with Ga-**D7**-^{124}I representing a notable exception: uptake in *P. aeruginosa* was significantly increased compared with ^{67}Ga-citrate and ^{67}Ga-**D7**, indicating a possibly increased affinity for transport receptors in *P. aeruginosa* (Figures S45 and 46, 5B, Tables S4–S6).

To determine if the bound activity is from active transporter-mediated uptake or nonspecific binding, we conducted an experiment with 200× of parent Fe-siderophore (Fe-LDFC for **D6** and Fe-DFO for **D7**) prior to the addition of ^{67}Ga-**D6**/**D7** conjugates. In accordance with active, siderophore transporter-mediated uptake, we observed a statistically significant decrease of ^{67}Ga-**D6**/**D7** uptake within the bacterial pellet at all time-points indicating siderophore-mediated specific uptake for ^{67}Ga-**D6**/**D7** (Figures S47–S52 and Tables S7–S12). This also indicates that nonspecific binding or precipitation effects affecting the observed uptake values can be excluded.

In Vivo Biodistribution and Pharmacokinetics in Mice.

With ^{67}Ga-**D6**-I, ^{67}Ga-**D7**-I, Ga-**D6**-^{124}I, Ga-**D7**-^{124}I, ^{67}Ga-**D6**, and ^{67}Ga-**D7** in vitro bacterial uptake assays complete, we investigated biodistribution of ^{67}Ga-**D6**/^{67}Ga-**D7** and Ga-**D6**-^{124}I/Ga-**D7**-^{124}I in vivo. Naive Balb/c mice were administered ^{67}Ga-**D6**, ^{67}Ga-**D7**, ^{67}Ga-citrate, Ga-**D6**-^{124}I, Ga-**D7**-^{124}I, and Tyrosine-^{124}I intravenously, followed by biodistribution and urine metabolite analysis using radio-HPLC at 1 h post-injection. Naive ^{67}Ga and ^{124}I biodistribution revealed rapid, renal clearance of all conjugates: ^{67}Ga-**D6**, ^{67}Ga-**D7**, ^{67}Ga-citrate, Ga-**D6**-^{124}I, Ga-**D7**-^{124}I, and Tyrosine-^{124}I (Figure 6A,D and Tables S14 and S15). In vivo biodistribution of Ga-**D6**-^{124}I, Ga-**D7**-^{124}I, and Tyrosine-^{124}I in a murine myositis with wt *S. aureus* produced no significant enhancement of uptake in the infected target muscle (Figures S53 and S54 and Tables S15–S16). It is likely that the structural impact of the tyrosine-modified linker impedes uptake as is indicated by the MIC assay results.

A urine metabolite analysis study revealed 5% intact detectable ^{67}Ga-**D6** (Figure 6B) and 0% intact ^{67}Ga-**D7** (Figure 6E), similar to our previous study. However, **D6**-^{124}I remained 45% intact (Figure 6C) while 64% of nondegraded **D7**-^{124}I was detected (Figure 6F). The differential metabolite profile of ^{67}Ga-**D6**/^{67}Ga-**D7** and Ga-**D6**-^{124}I/Ga-**D7**-^{124}I provides a strong indication that gallium dissociation is one of the primary sources of pharmacokinetic degradation in vivo due to the comparatively labile nature of Ga-LDFC and Ga-DFO complexes, while the ligand component experiences comparatively little degradation.

CONCLUSIONS

We show for the first time that a multi-isotope, radiochemical approach can be employed to elucidate the metabolic fate of the metal and the ligand component of Trojan horse conjugates comprising nonendogenous xenometal-chelating siderophores linked to antibiotics. Specifically, we demonstrate the feasibility of the tandem incorporation of the SPECT isotope ^{67}Ga by complexation and the PET isotope ^{124}I by covalent incorporation into the linker.

Two model xenometallomycins, Ga-**D6** and Ga-**D7**, as well as their iodinated analogues Ga-**D6**-I and Ga-**D7**-I were synthesized. Investigation of their antibiotic potency affirms that Ga-complexes exhibit improved growth inhibition when compared to their Fe- and *apo*-analogues. However, incorporation of tyrosine within the linker structure appears to have a detrimental effect on either siderophore recognition by transmembrane transporters or binding of the antibiotic ciprofloxacin to its cytoplasmic target. Radiochemical synthesis and subsequent purification produce ^{124}I- and ^{67}Ga-labeled constructs with high radiochemical purity for subsequent in vitro and in vivo assays. The ^{67}Ga-**D6** and ^{67}Ga-**D7** complexes show time-dependent siderophore-mediated active uptake in *wt* bacterial strains with an average uptake of ~20% for all strains tested. Ga-**D6**-^{124}I and Ga-**D7**-^{124}I displayed lower time-dependent uptake for *E. coli* and *P. aeruginosa* when compared to *S. aureus*. Biodistribution and urine metabolite analysis reveal significantly improved integrity of the radio-iodinated conjugate in contrast to the ^{67}Ga-labeled constructs.

In summary, Ga-**D6** and Ga-**D7** constitute the first xenometallomycins suitable for tagging with two short-lived biomedical isotopes. Direct isotope quantification also allows for a more comprehensive picture of siderophore-mediated internalization of antibiotic payloads, which can predict in vitro efficacy and enable the noninvasive identification, localization, and monitoring of bacterial infection in vivo. We anticipate the dual-isotope labeling strategy of xenometalsideromycins will further support antibiotic drug discovery efforts and improve understanding of structure–activity relationships of this emerging compound class.

MATERIALS AND METHODS

General.

All starting materials were purchased from Acros Organics, Alfa Aesar, Sigma-Aldrich, or TCI America and used without further purification. NMR spectra (^{1}H and ^{13}C) were collected on a 700 MHz, 500 MHz, or 400 MHz ADVANCE III Bruker instrument at 25 °C and processed using TopSpin 3.5pl7. ^{19}F NMR spectra were collected on a 400 MHz Bruker instrument at 25 °C using TFA as an internal standard (δ: −76 ppm). Chemical shifts are reported as parts per million (ppm). Mass spectrometry: low-resolution electrospray ionization (ESI) mass spectrometry and high-resolution (ESI) mass spectrometry was carried out at the Stony Brook University Institute for Chemical Biology and Drug Discovery (ICB&DD) Mass Spectrometry Facility with an Agilent LC/MSD and Agilent LC-UV-TOF spectrometers, respectively. UV–VIS spectra were collected with the NanoDrop 1C instrument (AZY1706045). Spectra were recorded from 190 to 850 nm in a quartz cuvette with a 1 cm path length. HPLC: Preparative HPLC was carried out using a Shimadzu HPLC-20AR equipped with a Binary Gradient, pump, UV–vis detector, manual injector on a Phenomenex Luna C18 column (250 mm × 21.2 mm, 100 Å, AXIA packed). Method A (preparative purification method): A = 0.1% TFA in water, B = 0.1% TFA in MeCN. Gradient: 0–5 min: 95% A. 5–24 min: 5–95% B gradient. Method B (preparative purification method): A = 10 mM sodium acetate (pH = 4.5) in water, B = 100% MeCN. Gradient: 0–5 min: 95% A. 5–24 min: 5–95% B gradient. Analytical HPLC analysis was carried out using a Shimadzu HPLC-20AR equipped with a binary gradient, pump, UV–vis detector, autoinjector, and Laura radio detector on a Phenomenex Luna C18 column (250

mm × 4 mm, 10 μm C18(2), 100 Å). Method C: A = 10 mM NaOAc (pH = 4.5), B = MeCN with a flow rate of 0.8 mL/min, UV detection at 254 and 280 nm. 0–2 min: 95% A. 2–5 min: 5–35% B. 5–23 min: 35–70%. 23–25 min:70–95%. Phenomenex Luna C18 column (150 mm × 3 mm, 100 Å, AXIA packed), method D (analysis of ^{67}Ga/Ga complexes): *A* = 10 mM sodium acetate (pH = 4.5) in water, *B* = 100% MeCN. Gradient: 0–2 min: 95% A. 2–14 min: 5–95% B. 14–16 min: 95% B. 16–16.6 min: 95–5% B. 16.5–20 min: 5% B, UV detection at 254 and 280 nm. Purity of all intermediates and final products including radiochemical species was determined using analytical HPLC. High-resolution (ESI) mass spectrometry was carried out at the Stony Brook University Institute for Chemical Biology and Drug Discovery (ICB&DD) Mass Spectrometry Facility with an Agilent LC/MSD and Agilent LC-UV-TOF spectrometers; low-resolution LC–MS was carried out using the Agilent 1260 Infinity II LC system and Agilent Infinity Lab LC/MSD system, single quadrupole, spray ionization with a Phenomenex Luna C18 column (150 mm × 3 mm, 100 Å, AXIA packed). *A* = 0.1% formic acid in water, *B* = 0.1% formic acid in MeCN with a flow rate of 0.8 mL/min, UV detection at 254 and 220 nm. Gradient, method E: 0–3 min: 5% B, 3–10: 5–95%B, 10–13 min: 95% B, 13–13.5 min: 95–5% B; 13.5–16 min: 5% B. All conjugates and complexes were ≥95% pure. ICP-OES was carried out using an Agilent 5110 ICP-OES. A 10-point standard with respect to gallium and iron was used, and lines of best fit were found with R2 of 0.999.5-(*N*-acetyl-*N*-acetoxyamino)-2-{5-(*N*-acetyl-*N*-acetoxy-amino)-2-[5-(*N*-acetyl-N acetoxyamino) -2-(benzyloxy-carbonylamino) valerylamino] valerylamino}valeric acid (**P5**) and 7-(4-*β*-Alanyl-1-piperazinyl)-1-cyclopropyl-6-fluoro-4-oxo-1*H*-quinoline-3-carboxylic acid (**B2**) were synthesized according to previously published procedures.[26] A detailed account of the chemical synthesis of **D6** and **D7**, including NMR spectral assignments, HPLC traces, HRMS, and corresponding data, is provided in the Supporting Information.

Synthesis of Coordination Complexes of D6 and D7.

Ga and Fe complexes of **D6** and **D7** were synthesized using the following protocol. **Ga-D6**. **D6** (0.010 g, 0.009 mmol, 1 equiv) was dissolved in DMF (1 mL), and $Ga(NO_3)_3$ (0.007 g, 0.027 mmol, 3 equiv) dissolved in 10 mM CH_3COONa (pH = 5) was added. The pH of the solution was adjusted to 6 by adding 0.1 M NaOH. The reaction mixture was stirred for 1 h at 60 °C and overnight at room temperature. The solvent was removed in vacuo and the product was purified by preparative HPLC (Method A, product elutes at 43% B) to afford Ga-**D6** (0.006 g, 0.005 mmol, 62%) as a white solid. Calculated mass for Ga-**D6** ($C_{50}H_{65}FGaN_{11}O_{15}$): 1147.3; found 1048.3 $[M + H]^+$. Retention time (Method D): 7.65 min (purity/peak area: > 99%). **Fe-D6**. **D6** (0.005 g, 0.004 mmol, 1 equiv) was dissolved in DMF (1 mL), and $FeCl_3$ (0.002 g, 0.012 mmol, 3 equiv) was added. The reaction mixture was stirred for 1 h at room temperature. The solvent was removed in vacuo, and the product was purified by preparative HPLC (Method A, product elutes at 48% B) to afford Fe-**D6** (0.006 g, 0.003 mmol, 87%) as a red solid. Calculated mass for Fe-**D6** ($C_{50}H_{65}FFeN_{11}O_{15}$): 1134.4; found 1135.4 $[M + H]^+$. Retention time (Method D): 7.48 min (purity/peak area: > 99%). **Ga-D7**. **D7** (7 mg, 0.006 mmol, 1 equiv) was dissolved in DMF (1 mL), and Ga $(NO_3)_3$ (5.1 mg, 0.018 mmol, 3 equiv) dissolved in 10 mM CH_3COONa (pH = 6) was added. The pH of the solution was adjusted to 6 by adding 1 M NaOH. The reaction mixture was stirred for 1 h at 60 °C and overnight at room temperature. The solvent was removed

in vacuo, and the product was purified by preparative HPLC (method D, product elutes at 50% B) to afford Ga-**D7** (0.0046 mmol, 5.6 mg, 78%) as a white solid. LC–MS: calculated mass for Ga-**D7** ($C_{55}H_{73}FGaN_{10}O_{15}$): 1202.46; found 1203.50 $[M + H]^+$. Retention time (method D): 8.19 min (purity/peak area: > 90%). **Fe-D7**. **D7** (4 mg, 0.0035 mmol, 1 equiv) was dissolved in DMF (1 mL), and $FeCl_3$ (0.0018 g, 0.011 mmol, 3 equiv) was added. The pH of the solution was adjusted to 6 by adding 1 M NaOH. The reaction mixture was stirred for 1 h at 60 °C and overnight at room temperature. The solvent was removed in vacuo, and the product was purified by preparative HPLC (method D, product elutes at 50% B) to afford Ga-**D7** (0.0048 mmol, 5.7 mg, 80%) as a white solid. LC–MS: calculated mass for Fe-**D7** ($C_{55}H_{74}FFeN_{10}O_{15}$): 1189.45; found 1190.40 $[M + H]^+$. Retention time (method D): 8.23 min (purity/peak area: > 90%).

Antimicrobial Activity Assay.

Antibacterial activity of *apo*-**D6** and **D7**, its corresponding Fe and Ga complexes, and iodinated Ga-**D6** and Ga-**D7** was determined by measuring their MICs using the broth microdilution method according to the Clinical and Laboratory Standards Institute (CLSI) guidelines. All aqueous solutions and media were prepared using deionized water. All liquids and media were sterilized by autoclaving (220 °C, 1 h) before use. Iron-deficient Mueller–Hinton broth (cation adjusted) was used for these assays. 5.25 g of MHB was added to 250 mL of deionized water. Aqueous solutions of 1 M Ca^{2+} (0.418 mL) and 1 M Mg^{2+} (0.155 mL) to 250 mL of MHB was added to the broth. The broth was autoclaved for 1 h at 220 °C. To make the broth iron-deficient, 4.06 mL of 1 mg/mL sterile (autoclaved) aq. solution of 2,2′-bipyridine (DP) was added to 250 mL of cation-adjusted MHB.

In general, 0.3 mM stock solution of testing compounds was prepared. 10 μL solution of testing compound (0.3 mM) was added to the first well of the 96-well plate and serial dilutions were made down each row of the plate. 40 μL of growth media and 50 μL of diluted bacterial inoculum were also added to each well, resulting in a total volume of 100 μL and a concentration gradient of 0.3×10^{-4} M to 0.92×10^{-12} M. The dilution rate was adjusted keeping in mind the MIC of ciprofloxacin (positive control). The plates were incubated at 37 °C for 13 h, and each plate was examined for bacterial growth using a plate reader (EPOCH2NS, Biotek microplate spectrometer). The MIC was recorded as the lowest compound concentration (μM) required to inhibit >90% of bacterial growth as judged by the absorbance of the culture media relative to the negative control.

Radiolabeling with ^{67}Ga.

^{67}Ga-citrate was received from Jubilant Radiopharma at an average specific activity of 140.9 MBq/mL. The ^{67}Ga-citrate solution was converted to ^{67}Ga-chloride using a previously described protocol. The average specific activity of the resultant ^{67}Ga-chloride solution used for radiolabeling was 137.2 MBq/mL. For radiolabeling of **D6** and **D7**, an aliquot of $^{67}GaCl_3$ (2.3 MBq, 15 μL) was mixed with a solution of **D6** (50 μL, 0.01 mM) and an aliquot of $^{67}GaCl_3$ (3.2 MBq, 30 μL) was mixed with a solution **D7**(40 μL, 0.003 mM). The pH of the solution was adjusted with HEPES (100 mM, 80 μL) to 7.4. Complexation was monitored by radio-HPLC, method D. Radiolabeling was found to proceed after 5 min at room temperature. The conjugates were purified with HPLC to isolate the desired

radiolabeled product using method C. Radiochemical yield: >99%. ^{67}Ga-**D6**: R_t = 7.50 min (purity/peak area: 99%). ^{67}Ga-**D7:** R_t = 8.11 min (purity/peak area: 99%). For radiolabeling **D6**-I, $^{67}GaCl_3$ (4.3 MBq, 20 μL) was mixed with a solution of **D6-I** (10 μL, 0.01 mM) in chelex resin-treated water. The pH of the solution was adjusted with HEPES (100 mM, 40 μL) to 7.4. Complexation was monitored by radio-HPLC, method D. For **D7**-I, $^{67}GaCl_3$ (4.3 MBq, 20 μL) was mixed with a solution of **D7**-I (45 μL, 1.5 mM). Radiolabeling was found to proceed after 5 min at room temperature. Radiochemical yield: ~10%. ^{67}Ga-**D6**-I: R_t = 7.90 min (purity/peak area: 99%). ^{67}Ga-**D7**-I: Radiochemical yield ~15%, R_t = 7.93 min (purity/peak area: >95%).

Bacterial Uptake of ^{67}Ga in wt Bacterial Strains.

wt *E. coli* (Mg 1655), wt *S. aureus* (RN4220), and wt *P. aeruginosa* (PAO1) were grown overnight in 5 mL LB (Fe-deficient) at 37 °C. The overnight cultures were inoculated in 10 mL iron-deficient LB and incubated at 37 °C until the OD_{600} reached 0.4. Uptake was initiated by adding ^{67}Ga complexes (10 μL, 0.11 MBq) to culture tubes containing 10 mL bacterial inoculum and incubating at 37 °C. Aliquots (1 mL) were removed after 10, 20, 30 min, 1, and 2 h and centrifuged for 3 min (34 000 rpm). The supernatant was removed, and the bacterial pellet was washed with DPBS (1 mL, 3×). The assay was performed in five replicates and in parallel with a ^{67}Ga-citrate control. All tubes were counted using an automated gamma counter to quantify retained radioactivity in pellets in comparison to the 1 mL parent inoculum.

Radiolabeling with ^{124}I.

^{124}I was received from 3D imaging at an average specific activity of 17131 MBq/mL, as an aqueous solution of NaOH. The stock solution was diluted with 100 μL water. The average specific activity of the resultant ^{124}I solution used for radiolabeling was 3515 MBq/mL. Direct radioiodination was carried out using Iodo-gen-precoated iodination test tubes (Pierce 28601) at pH = 7.4, 25 °C for 45 min. In general, stock solutions of Tyrosine, Ga-**D6,** and Ga-**D7** dissolved in buffer (HEPES, 100 mM, 100 μL) were added to the iodo-gen tube. An aliquot of ^{124}I (9.5 MBq, 3 μL) was added to the tube. The sample was vortexed for 5 min and incubated at room temperature. After 45 min, the conjugates were purified on radio HPLC to isolate the mono-iodinated product using method C. Radiochemical yield 15–20%. Tyrosine-^{124}I: t_R = 4.97 min, Ga-**D6**-^{124}I: t_R = 8.40 min, and Ga-**D7**-^{124}I: t_R = 8.73 min (purity/peak area: 99%).

Bacterial Uptake of ^{124}I in wt Bacterial Strains.

wt *E. coli* (Mg 1655), wt *S. aureus* (RN4220), and wt *P. aeruginosa* (PAO1) were grown overnight in 5 mL LB (Fe-deficient) at 37 °C. The overnight cultures were inoculated in 10 mL iron-deficient LB and incubated at 37 °C until the OD_{600} reached 0.4. Uptake was initiated by adding ^{124}I complexes (10 μL, 0.14 MBq) to culture tubes containing 10 mL bacterial inoculum and incubating at 37 °C. Aliquots (1 mL) were removed after 10, 20, 30 min, 1, and 2 h and centrifuged for 3 min (34 000 rpm). The supernatant was removed, and the bacterial pellet was washed with DPBS (1 mL, 3×). The assay was performed in five replicates and in parallel with a tyrosine-^{124}I control. All tubes were counted using an

automated gamma counter to quantify retained radioactivity in pellets in comparison to the 1 mL parent inoculum.

Biodistribution of Naive Balb/C Mice.

All animal experiments were performed using protocols approved by the Institutional Animal Care and Use Committee (IACUC) at Stony Brook University accredited through the Association for Assessment and Accreditation of Laboratory Animal Care International (AAALAC International, Federal assurance #A3011–01). 0.5–0.7 MBq of ^{67}Ga-**D6**, ^{67}Ga-**D7**, and ^{67}Ga-citrate (control) and 0.2–0.4 MBq of Ga-**D6**-^{124}I, Ga-**D7**-^{124}I, and Tyrosine-^{124}I (control) were intravenously injected via tail vein catheter in naive mice. Mice were sacrificed 1 h p.i., and select organs were harvested. Radioactivity was counted by using a gamma counter, and the radioactivity associated with each organ was expressed as % ID/g.

Biodistribution of Infected Balb/C Mice.

Murine myositis models were established by intramuscular (i.m.) injection of live or heat-killed (90 °C, 30 min) strains of wt *S. aureus*. Mice were inoculated with 10^8 cfus of wt *S. aureus* in the right triceps and with a tenfold higher (10^9) burden of heat-killed bacteria on the left triceps. The microbial infections were allowed to develop for 5 h. Subsequently, 0.2–0.4 MBq of Ga-**D6**-^{124}I and Tyrosine-^{124}I (control) was injected. Mice were sacrificed 1 h p.i., and select organs were harvested. Radioactivity was counted by using a gamma counter, and the radioactivity associated with each organ was expressed as % ID/g.

Metabolite Analysis.

100 μL of urine was directly injected on radio HPLC. Eluate was collected in 30 s increments from 0–15 min. Activity in each tube was quantified using a gamma counter. The counts were used to reconstruct the metabolite trace, which was then compared to the HPLC traces of the original ^{67}Ga-**D6**, ^{67}Ga-**D7**, Ga-**D6**-^{124}I, and Ga-**D7**-^{124}I complexes.

Supplementary Material

Refer to Web version on PubMed Central for supplementary material.

ACKNOWLEDGMENTS

We thank Peter Tonge and members of his research group, specifically Dr. Yong Li for granting access to *wt* bacterial strains.

Funding

E.B. acknowledges the National Institutes for General Medicine (NIGMS) are for funding (R35GM142770). M.C. acknowledges a fellowship provided by the Chemical Biology Training program (T32GM136572).

REFERENCES

(1). CDC. Biggest Threats and Data | Antibiotic/Antimicrobial Resistance; CDC, 2019.

(2). National Institute of Allergy and Infectious Diseases. Causes of Antimicrobial (Drug) Resistance | NIH; National Institute of Allergy and Infectious Diseases, 2011.

(3). Webber MA; Piddock LJV The Importance of Efflux Pumps in Bacterial Antibiotic Resistance. J. Antimicrob. Chemother 2003, 51, 9–11. [PubMed: 12493781]

(4). Alcalde-Rico M; Hernando-Amado S; Blanco P; Martïnez JL Multidrug Efflux Pumps at the Crossroad between Antibiotic Resistance and Bacterial Virulence. Front. Microbiol 2016, 7, 1483. [PubMed: 27708632]

(5). Nikaido H Prevention of Drug Access to Bacterial Targets: Permeability Barriers and Active Efflux. Science 80- 1994, 264, 382–388.

(6). Poole K Efflux-Mediated Antimicrobial Resistance. J. Antimicrob. Chemother 2005, 56, 20–51. [PubMed: 15914491]

(7). Ji C; Juárez-Hernández RE; Miller MJ Exploiting Bacterial Iron Acquisition: Siderophore Conjugates. Future Med. Chem 2012, 4, 297–313. [PubMed: 22393938]

(8). Wencewicz TA; Miller MJ Sideromycins as Pathogen-Targeted Antibiotics. Top. Med. Chem 2018, 26, 151–183.

(9). Miller MJ; Zhu H; Xu Y; Wu C; Walz AJ; Vergne A; Roosenberg JM; Moraski G; Minnick AA; McKee-Dolence J; Hu J; Fennell K; Kurt Dolence E; Dong L; Franzblau S; Malouin F; Möllmann U Utilization of Microbial Iron Assimilation Processes for the Development of New Antibiotics and Inspiration for the Design of New Anticancer Agents. BioMetals 2009, 22, 61–75. [PubMed: 19130268]

(10). Ji C; Miller MJ Siderophore-Fluoroquinolone Conjugates Containing Potential Reduction-Triggered Linkers for Drug Release: Synthesis and Antibacterial Activity. BioMetals 2015, 28, 541–551. [PubMed: 25663417]

(11). Roosenberg JM II; Lin Y-M; Lu Y; Miller M Studies and Syntheses of Siderophores, Microbial Iron Chelators, and Analogs as Potential Drug Delivery Agents. Curr. Med. Chem 2012, 7, 159–197.

(12). Wencewicz TA; Miller MJ Biscatecholate-Monohydroxamate Mixed Ligand Siderophore-Carbacephalosporin Conjugates Are Selective Sideromycin Antibiotics That Target Acinetobacter Baumannii. J. Med. Chem 2013, 56, 4044–4052. [PubMed: 23614627]

(13). Miller MJ; Malouin F Microbial Iron Chelators as Drug Delivery Agents: The Rational Design and Synthesis of Siderophore-Drug Conjugates. Acc. Chem. Res 1993, 26, 241–249.

(14). Dolence EK; Minnick AA; Miller MJ N5-Acetyl-N5-hydroxy-L-ornithine-derived siderophore-carbacephalosporin .beta.-lactam conjugates: iron transport mediated drug delivery. J. Med. Chem 1990, 33, 461–464. [PubMed: 2137180]

(15). Ghosh M; Lin Y-M; Miller PA; Möllmann U; Boggess WC; Miller MJ Siderophore Conjugates of Daptomycin Are Potent Inhibitors of Carbapenem Resistant Strains of Acinetobacter Baumannii. ACS Infect. Dis 2018, 4, 1529–1535. [PubMed: 30043609]

(16). Johnstone TC; Nolan EM Beyond Iron: Non-Classical Biological Functions of Bacterial Siderophores. Dalton Trans 2015, 44, 6320–6339. [PubMed: 25764171]

(17). Zheng T; Bullock JL; Nolan EM Siderophore-Mediated Cargo Delivery to the Cytoplasm of Escherichia Coli and Pseudomonas Aeruginosa: Syntheses of Monofunctionalized Enterobactin Scaffolds and Evaluation of Enterobactin-Cargo Conjugate Uptake. J. Am. Chem. Soc 2012, 134, 18388–18400. [PubMed: 23098193]

(18). Neumann W; Nolan EM Evaluation of a Reducible Disulfide Linker for Siderophore-Mediated Delivery of Antibiotics. J. Biol. Inorg Chem 2018, 23, 1025–1036. [PubMed: 29968176]

(19). Neumann W; Sassone-Corsi M; Raffatellu M; Nolan EM Esterase-Catalyzed Siderophore Hydrolysis Activates an Enterobactin-Ciprofloxacin Conjugate and Confers Targeted Antibacterial Activity. J. Am. Chem. Soc 2018, 140, 5193–5201. [PubMed: 29578687]

(20). Zheng T; Nolan EM Enterobactin-Mediated Delivery of β-Lactam Antibiotics Enhances Antibacterial Activity against Pathogenic Escherichia coli. J. Am. Chem. Soc 2014, 136, 9677–9691. [PubMed: 24927110]

(21). Ferreira K; Hu H-Y; Fetz V; Prochnow H; Rais B; Müller PP; Brönstrup M Multivalent Siderophore-DOTAM Conjugates as Theranostics for Imaging and Treatment of Bacterial Infections. Angew. Chem., Int. Ed 2017, 56, 8272–8276.

(22). Milner SJ; Seve A; Snelling AM; Thomas GH; Kerr KG; Routledge A; Duhme-Klair A-K Staphyloferrin A as Siderophore-Component in Fluoroquinolone-Based Trojan Horse Antibiotics. Org. Biomol. Chem 2013, 11, 3461–3468. [PubMed: 23575952]

(23). Sanderson TJ; Black CM; Southwell JW; Wilde EJ; Pandey A; Herman R; Thomas GH; Boros E; Duhme-Klair A-K; Routledge A A Salmochelin S4-Inspired Ciprofloxacin Trojan Horse Conjugate. ACS Infect. Dis 2020, 6, 2532–2541. [PubMed: 32786274]

(24). Milner SJ; Snelling AM; Kerr KG; Abd-El-Aziz A; Thomas GH; Hubbard RE; Routledge A; Duhme-Klair A-K Probing Linker Design in Citric Acid-Ciprofloxacin Conjugates. Bioorg. Med. Chem 2014, 22, 4499–4505. [PubMed: 24794750]

(25). Wencewicz TA; Long TE; Möllmann U; Miller MJ Trihydroxamate Siderophore-Fluoroquinolone Conjugates Are Selective Sideromycin Antibiotics That Target Staphylococcus Aureus. Bioconjugate Chem 2013, 24, 473–486.

(26). Pandey A; Savino C; Ahn SH; Yang Z; Van Lanen SG; Boros E Theranostic Gallium Siderophore Ciprofloxacin Conjugate with Broad Spectrum Antibiotic Potency. J. Med. Chem 2019, 62, 9947–9960. [PubMed: 31580658]

(27). Pandey A; Śmiłowicz D; Boros E Galbofloxacin: A Xenometal-Antibiotic with Potentin Vitroandin Vivoefficacy AgainstS. Aureus. Chem. Sci 2021, 12, 14546–14556. [PubMed: 34881006]

(28). Lin Z; Xu X; Zhao S; Yang X; Guo J; Zhang Q; Jing C; Chen S; He Y Total Synthesis and Antimicrobial Evaluation of Natural Albomycins against Clinical Pathogens. Nat. Commun 2018, 9, 3445. [PubMed: 30181560]

(29). Braun V; Pramanik A; Gwinner T; Köberle M; Bohn E Sideromycins: Tools and Antibiotics. BioMetals 2009, 22, 3–13. [PubMed: 19130258]

(30). Dong L; Roosenberg JM; Miller MJ Total Synthesis of Desferrisalmycin B. J. Am. Chem. Soc 2002, 124, 15001–15005. [PubMed: 12475343]

(31). Caudy AA; Hanchard JA; Hsieh A; Shaan S; Rosebrock AP Functional Genetic Discovery of Enzymes Using Full-Scan Mass Spectrometry Metabolomics. Biochem. Cell Biol 2019, 97, 73–84. [PubMed: 30001498]

(32). Zampieri M; Zimmermann M; Claassen M; Sauer U Nontargeted Metabolomics Reveals the Multilevel Response to Antibiotic Perturbations. Cell Rep 2017, 19, 1214–1228. [PubMed: 28494870]

(33). Zampieri M; Szappanos B; Buchieri MV; Trauner A; Piazza I; Picotti P; Gagneux S; Borrell S; Gicquel B; Lelievre J; Papp B; Sauer U High-Throughput Metabolomic Analysis Predicts Mode of Action of Uncharacterized Antimicrobial Compounds. Sci. Transl. Med 2018, 10, No. eaal3973. [PubMed: 29467300]

(34). Hoerr V; Duggan GE; Zbytnuik L; Poon KKH; Große C; Neugebauer U; Methling K; Löffler B; Vogel HJ Characterization and Prediction of the Mechanism of Action of Antibiotics through NMR Metabolomics. BMC Microbiol 2016, 16, 82. [PubMed: 27159970]

(35). Stintzi A; Barnes C; Xu J; Raymond KN Microbial Iron Transport via a Siderophore Shuttle: A Membrane Ion Transport Paradigm. Proc. Natl. Acad. Sci. U.S.A 2000, 97, 10691–10696. [PubMed: 10995480]

(36). Tufano TP; Raymond KN Coordination Chemistry of Microbial Iron Transport Compounds. 21. Kinetics and Mechanism of Iron Exchange in Hydroxamate Siderophore Complexes. J. Am. Chem. Soc 1981, 103, 6617–6624.

(37). Ecker DJ; Matzanke BF; Raymond KN Recognition and Transport of Ferric Enterobactin in Escherichia Coli. J. Bacteriol 1986, 167, 666–673. [PubMed: 2942532]

(38). Gasser V; Baco E; Cunrath O; August PS; Perraud Q; Zill N; Schleberger C; Schmidt A; Paulen A; Bumann D; Mislin GL; Schalk IJ Catechol Siderophores Repress the Pyochelin Pathway and Activate the Enterobactin Pathway in Pseudomonas Aeruginosa: An Opportunity for Siderophore-Antibiotic Conjugates Development. Environ. Microbiol 2016, 18, 819–832. [PubMed: 26718479]

(39). Petrik M; Haas H; Dobrozemsky G; Lass-Flörl C; Helbok A; Blatzer M; Dietrich H; Decristoforo C 68Ga-Siderophores for PET Imaging of Invasive Pulmonary Aspergillosis: Proof of Principle. J. Nucl. Med 2010, 51, 639–645. [PubMed: 20351354]

(40). Petrik M; Umlaufova E; Raclavsky V; Palyzova A; Havlicek V; Haas H; Novy Z; Dolezal D; Hajduch M; Decristoforo C Imaging of Pseudomonas Aeruginosa Infection with Ga-68 Labelled Pyoverdine for Positron Emission Tomography. Sci. Rep 2018, 8, 15698. [PubMed: 30356077]

(41). Petrik M; Zhai C; Novy Z; Urbanek L; Haas H; Decristoforo C Vitro and In Vivo Comparison of Selected Ga-68 and Zr-89 Labelled Siderophores. Mol. Imaging Biol 2016, 18, 344–352. [PubMed: 26424719]

(42). Petrik M; Haas H; Schrettl M; Helbok A; Blatzer M; Decristoforo C In vitro and in vivo evaluation of selected 68Ga-siderophores for infection imaging. Nucl. Med. Biol 2012, 39, 361–369. [PubMed: 22172389]

(43). Petrik M; Zhai C; Haas H; Decristoforo C Siderophores for Molecular Imaging Applications. Clin. Trans. Imag 2017, 5, 15–27.

(44). Kuker R; Sztejnberg M; Gulec S I-124 Imaging and Dosimetry. Mol. Imaging Radionucl. Ther 2017, 26, 66–73. [PubMed: 28117290]

(45). Moroz MA; Serganova I; Zanzonico P; Ageyeva L; Beresten T; Dyomina E; Burnazi E; Finn RD; Doubrovin M; Blasberg RG Imaging HNET Reporter Gene Expression with 124I-MIBG. J. Nucl. Med 2007, 48, 827–836. [PubMed: 17475971]

(46). Cistaro A; Quartuccio N; Caobelli F; Piccardo A; Paratore R; Coppolino P; Sperandeo A; Arnone G; Ficola U 124I-MIBG: A New Promising Positron-Emitting Radiopharmaceutical for the Evaluation of Neuroblastoma. Nucl. Med. Rev 2015, 18, 102–106.

(47). Schneider RF; Engelhardt EL; Stobbe CC; Fenning MC; Chapman JD The Synthesis and Radiolabeling of Novel Markers of Tissue Hypoxia of the Iodinated Azomycin Nucleoside Class. J. Label. Compd. Radiopharm 1997, 39, 541–557.

(48). Riedl CC; Brader P; Zanzonico P; Reid V; Woo Y; Wen B; Ling CC; Hricak H; Fong Y; Humm JL Tumor Hypoxia Imaging in Orthotopic Liver Tumors and Peritoneal Metastasis: A Comparative Study Featuring Dynamic 18F-MISO and 124I-IAZG PET in the Same Study Cohort. Eur. J. Nucl. Med. Mol. Imag 2008, 35, 39–46.

(49). Riedl CC; Brader P; Zanzonico PB; Chun YS; Woo Y; Singh P; Carlin S; Wen B; Ling CC; Hricak H; Fong Y Imaging Hypoxia in Orthotopic Rat Liver Tumors with Iodine 124-Labeled Iodoazomycin Galactopyranoside PET. Radiology 2008, 248, 561–570. [PubMed: 18641253]

(50). Stahlschmidt A; Machulla HJ; Reischl G; Knaus EE; Wiebe LI Radioiodination of 1-(2-Deoxy-β-d-Ribofuranosyl)-2,4-Difluoro-5-Iodobenzene (DRFIB), a Putative Thymidine Mimic Nucleoside for Cell Proliferation Studies. Appl. Radiat. Isot 2008, 66, 1221–1228. [PubMed: 18662615]

(51). Bettegowda C; Foss CA; Cheong I; Wang Y; Diaz L; Agrawal N; Fox J; Dick J; Dang LH; Zhou S; Kinzler KW; Vogelstein B; Pomper MG Imaging Bacterial Infections with Radiolabeled 1-(2′-Deoxy-2′- Fluoro-β-D-Arabinofuranosyl)-5-Iodouracil. Proc. Natl. Acad. Sci. U.S.A 2005, 102, 1145–1150. [PubMed: 15653773]

(52). Koziorowski J; Henssen C; Weinreich R A New Convenient Route to Radioiodinated N-Succinimidyl 3- and 4- Iodobenzoate, Two Reagents for Radioiodination of Proteins. Appl. Radiat. Isot 1998, 49, 955–959.

(53). Robinson MK; Doss M; Shaller C; Narayanan D; Marks JD; Adler LP; González Trotter DE; Adams GP Quantitative Immuno-Positron Emission Tomography Imaging of HER2-Positlve Tumor Xenografts with an Iodine-124 Labeled Anti-HER2 Diabody. Cancer Res 2005, 65, 1471–1478. [PubMed: 15735035]

(54). Behr TM; Gotthardt M; Becker W; Béhé M Radioiodination of Monoclonal Antibodies, Proteins and Peptides for Diagnosis and Therapy: A Review of Standardized, Reliable and Safe Procedures for Clinical Grade Levels KBq to GBq in the Göttingen/Marburg Experience. NuklearMedizin 2002, 41, 71–79. [PubMed: 11989301]

(55). Salacinski PRP; McLean C; Sykes JEC; Clement-Jones VV; Lowry PJ Iodination of Proteins, Glycoproteins, and Peptides Using a Solid-Phase Oxidizing Agent, 1,3,4,6-Tetrachloro-3α,6α-Diphenyl Glycoluril (Iodogen). Anal. Biochem 1981, 117, 136–146. [PubMed: 7316186]

(56). Dolence EK; Minnick AA; Lin CE; Miller MJ; Payne SM Synthesis and Siderophore and Antibacterial Activity of N5-Acetyl-N5-Hydroxy-L-Ornithine-Derived Siderophore-β-Lactam

Conjugates: Iron-Transport-Mediated Drug Delivery. J. Med. Chem 1991, 34, 968–978. [PubMed: 1825850]

(57). Adams CJ; Wilson JJ; Boros E Multifunctional Desferrichrome Analogues as Versatile 89 Zr(IV) Chelators for ImmunoPET Probe Development. Mol. Pharm 2017, 14, 2831–2842. [PubMed: 28665620]

(58). Juárez-Hernández RE; Miller PA; Miller MJ Syntheses of Siderophore-Drug Conjugates Using a Convergent Thiol-Maleimide System. ACS Med. Chem. Lett 2012, 3, 799–803. [PubMed: 23264853]

(59). Hunsaker EW; Franz KJ Emerging Opportunities to Manipulate Metal Trafficking for Therapeutic Benefit. Inorg. Chem 2019, 58, 13528–13545. [PubMed: 31247859]

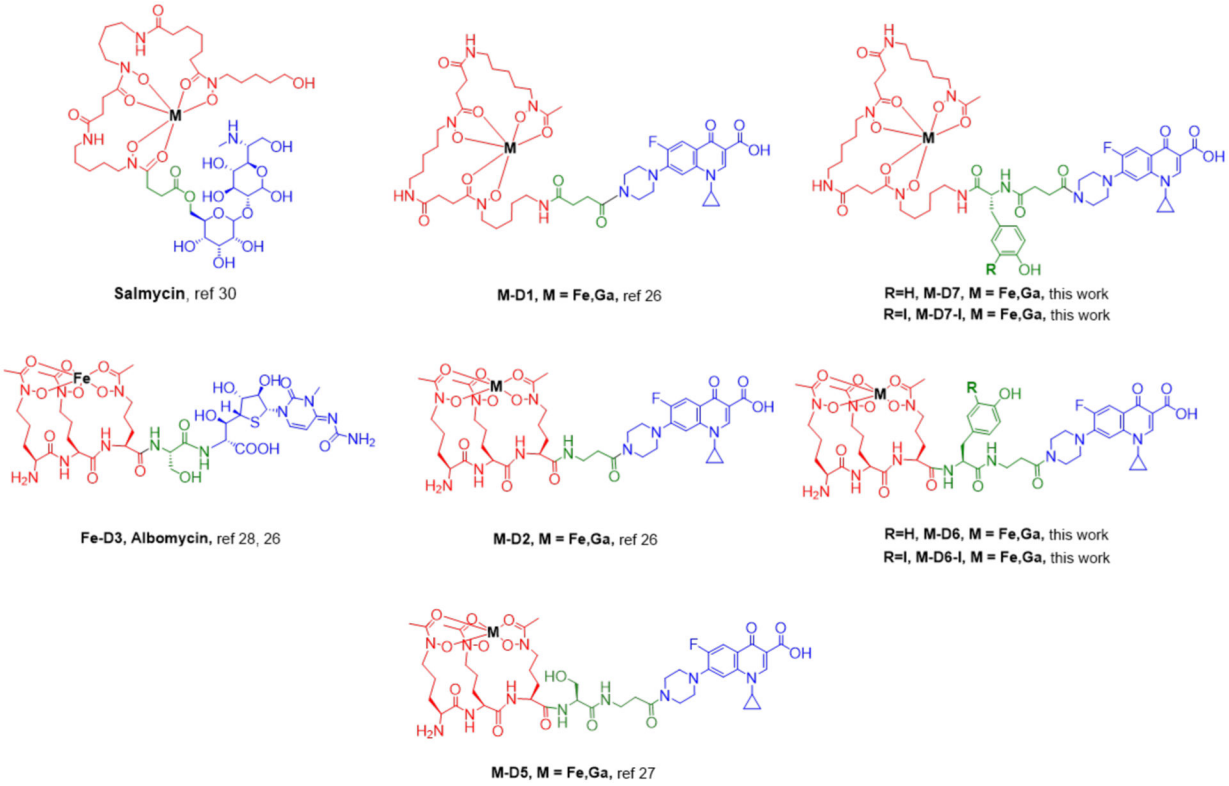

Figure 1.

Chemical structures of relevant natural products, previously described desferrioxamine (DFO) siderophore–antibiotic conjugates investigated by us, as well as the compounds described in this work. Black: Metal ion, red: siderophore, green: linker, and blue: antibiotic.

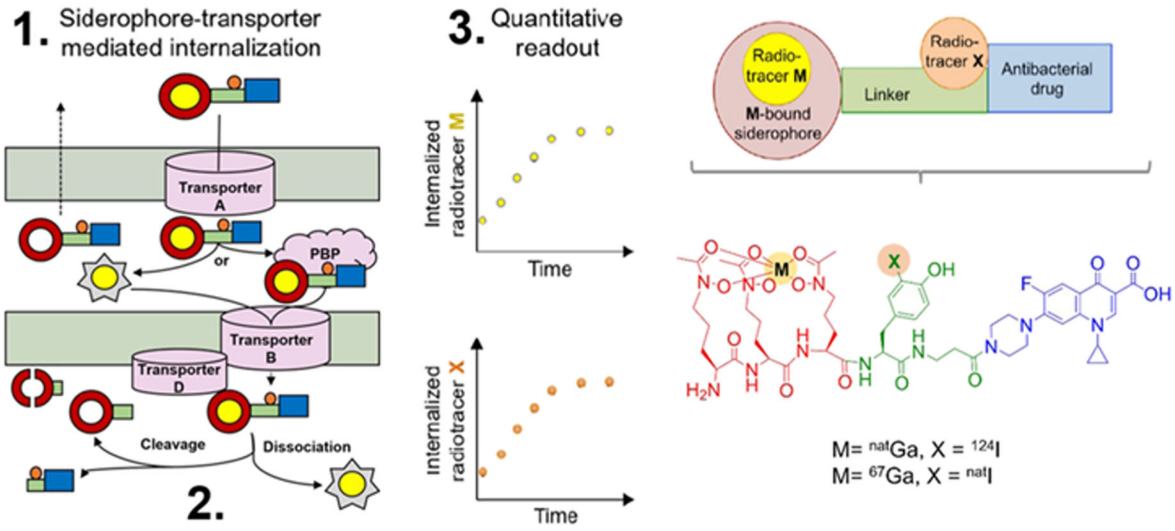

Figure 2.

(1) Proposed internalization pathways for the siderophore antibiotic construct. (2) Periplasm or cytoplasmic metabolism, leading to direct quantification of isotope internalization in a Gram-negative bacterium; periplasmic binding protein PBP. (3) Siderophore antibiotic conjugate implementing the dual tracer strategy to study the in vitro and in vivo behavior of siderophore antibiotic conjugates.

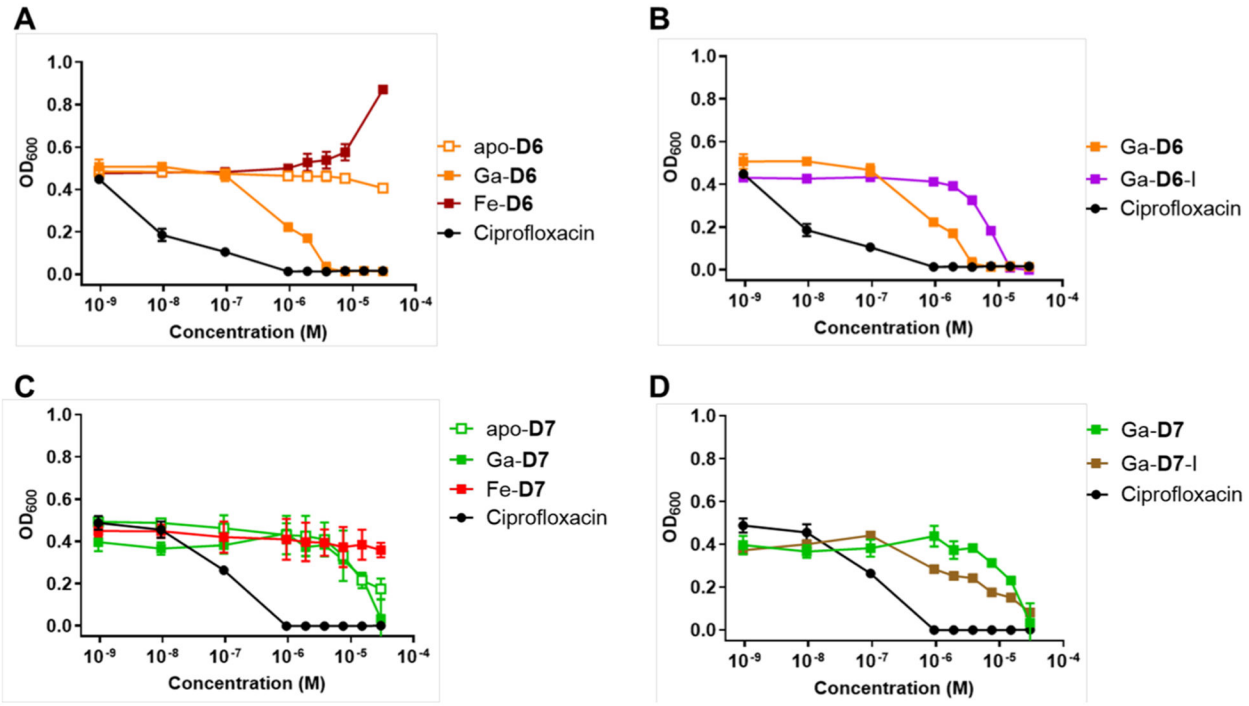

Figure 3.

(A) MIC assay of **D6** and its complexes in *S. aureus* (n = 9). (B) MIC assay of Ga-**D6**-I in *S. aureus* shows fivefold lower potency as compared with Ga-**D6** (*n* = 9). (C) MIC assay of **D7** and its complexes in *S. aureus* (*n* = 9). (D) MIC assay of Ga-**D7**-I in *S. aureus* shows comparable potency with Ga-**D7** (*n* = 9).

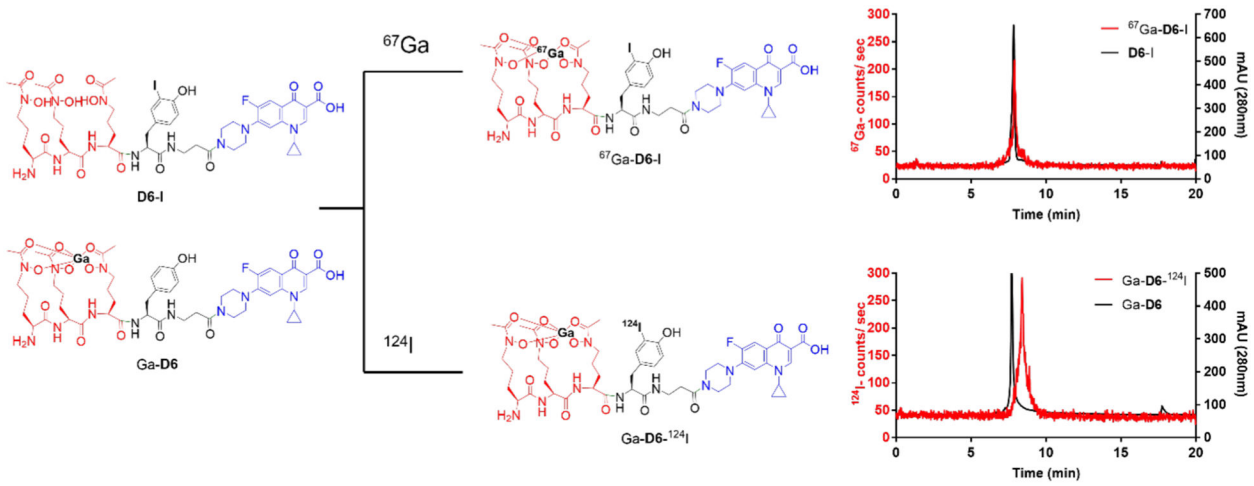

Figure 4.

(Top) Schematic description of the radiochemical complexation of **D6**-I with ^{67}Ga. ^{67}Ga-complexation proceeds in 5 min, 25 °C, pH 7. A representative radiolabeling of the HPLC trace for the characterization of ^{67}Ga-**D6**-I (t_R = 7.90 min, left axis, ^{67}Ga counts per second, method D), in comparison with HPLC characterization of the **D6**-I ligand (t_R = 7.83 min, right axis, absorbance at 280 nm, method D) is shown. Free ^{67}Ga elutes at 0.7 min (Bottom) Schematic description of the radiolabeling of Ga-**D6** with ^{124}I. A representative radiolabeling HPLC trace for the characterization of Ga-**D6**-^{124}I (t_R = 8.40 min, left axis, ^{124}I counts per second, method C), in comparison with HPLC characterization of the Ga-**D6** ligand (t_R = 7.77 min, right axis, absorbance at 280 nm, method C) is shown. Free ^{124}I elutes at 1.03 min.

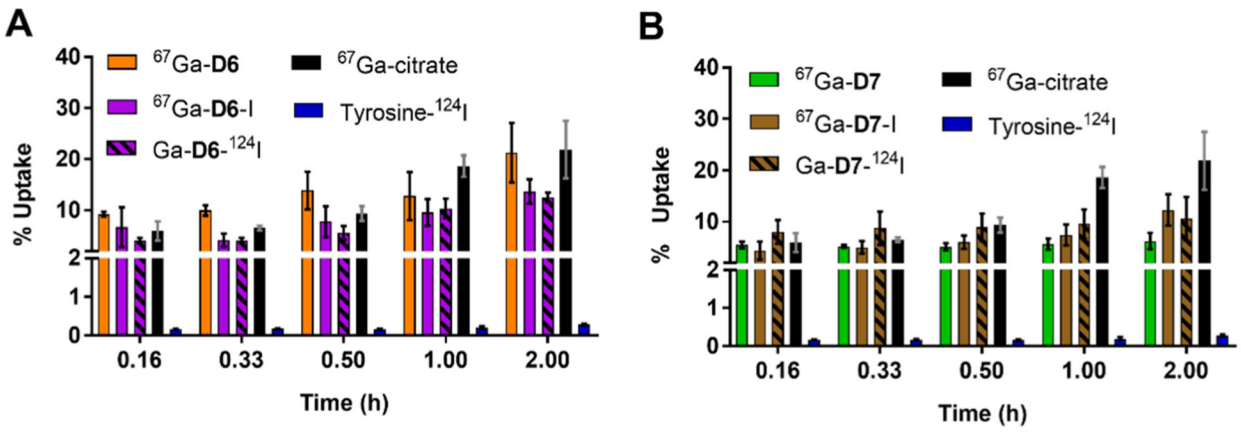

Figure 5.

(A) Time-dependent, radiochemical bacterial uptake studies in *S. aureus* RN4220 of ^{67}Ga-**D6**, ^{67}Ga-**D6**-I, and Ga-**D6**-^{124}I in iron-depleted, DP-treated media, pH = 7.4 with controls ^{67}Ga-citrate and Tyrosine-^{124}I ($n = 5 \times 3$). (B) Time-dependent, radiochemical bacterial uptake studies in *S. aureus* RN4220 of ^{67}Ga-**D7**, ^{67}Ga-**D7**-I, and Ga-**D7**-^{124}I in iron-depleted, DP-treated media, pH = 7.4 with controls ^{67}Ga-citrate and Tyrosine-^{124}I ($n = 5 \times 3$). Quantitation based on radioactive uptake normalized to the total activity used per sample.

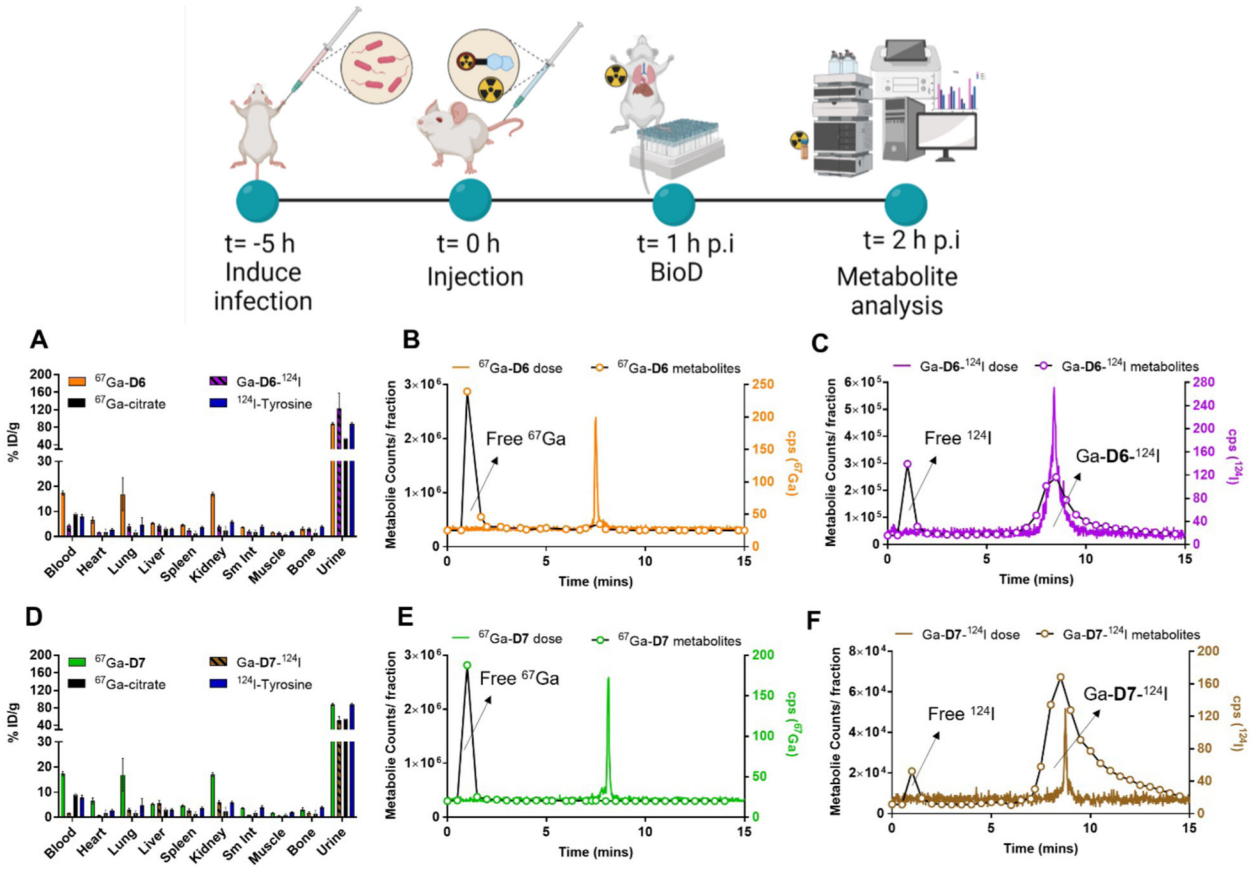

Figure 6.

(Top panel) Animal study experimental timeline. (A) Comparative biodistribution of ^{67}Ga-**D6**, ^{67}Ga-citrate, Ga-**D6**-^{124}I, and Tyrosine-^{124}I in naive mice (n = 3) shows a rapid renal clearance and no major off-target uptake. **(B)** Metabolite analysis of ^{67}Ga-**D6** (open circles) shows a detectable intact complex (5%) in the urine 1 h post-injection. Radioanalytical HPLC trace of the ^{67}Ga-**D6** dose formulation prior to administration is shown as a reference (orange). (C) Metabolite analysis of Ga-**D6**-^{124}I (open circles) shows a detectable intact complex (45%) in the urine 1 h post-injection. Radioanalytical HPLC trace of the ^{124}I-Ga-**D6** dose formulation prior to administration is shown as a reference (purple). (D) Comparative biodistribution of ^{67}Ga-**D7**, ^{67}Ga-citrate, Ga-**D7**-^{124}I, and Tyrosine-^{124}I in naive mice (n = 3) shows rapid renal clearance and no major off-target uptake. (E) Metabolite analysis of ^{67}Ga-**D7** (open circles) shows 0% intact complex in the urine 1 h post-injection. Radioanalytical HPLC trace of the ^{67}Ga-**D7** dose formulation prior to administration is shown as a reference (green). (F) Metabolite analysis of Ga-**D7**-^{124}I (open circles) shows detectable intact complex (64%) in the urine 1 h post-injection. Radioanalytical HPLC trace of the Ga-**D7**-^{124}I dose formulation prior to administration is shown as a reference (brown).

Table 1.

Summary of MIC (μM) Determined in *E. coli*, *S. aureus*, and *P. aeruginosa*[a]

Compound	*E. coli*	*S. aureus*	*PA01*
ciprofloxacin	0.93	0.93	0.93
apo-**D6**	Inactive	Inactive	Inactive
Ga-**D6**	1.9	3.8	Inactive
Fe-**D6**	Inactive	GP	Inactive
Ga-**D6-I**	30	15	ND
apo-**D7**	Inactive	Inactive	Inactive
Ga-**D7**	30	30	Inactive
Fe-**D7**	GP	Inactive	GP
Ga-**D7-I**	Inactive	Inactive	ND
Ga-**D1**	1.9	0.002	15
Ga-**D2**	0.23	0.94	3.8

[a]GP: growth promoting. ND: not determined.